

Adversarial Attacks on Medical Hyperspectral Imaging Exploiting Spectral-Spatial Dependencies and Multiscale Features

Yunrui Gu, Zhenzhe Gao, Cong Kong, Zhaoxia Yin

Abstract—Medical hyperspectral imaging (HSI) enables accurate disease diagnosis by capturing rich spectral-spatial tissue information, but recent advances in deep learning have exposed its vulnerability to adversarial attacks. In this work, we identify two fundamental causes of this fragility: the reliance on local pixel dependencies for preserving tissue structure and the dependence on multiscale spectral-spatial representations for hierarchical feature encoding. Building on these insights, we propose a targeted adversarial attack framework for medical HSI, consisting of a Local Pixel Dependency Attack that exploits spatial correlations among neighboring pixels, and a Multiscale Information Attack that perturbs features across hierarchical spectral-spatial scales. Experiments on the Brain and MDC datasets demonstrate that our attacks significantly degrade classification performance, especially in tumor regions, while remaining visually imperceptible. Compared with existing methods, our approach reveals the unique vulnerabilities of medical HSI models and underscores the need for robust, structure-aware defenses in clinical applications.

Index Terms—medical hyperspectral, adversarial attack, spectral-spatial dependency, multiscale features

I. INTRODUCTION

Hyperspectral imaging (HSI) is a powerful technique that captures a wide spectrum of light across contiguous bands, enabling detailed analysis of material and surface characteristics. Originally developed for agriculture, environmental monitoring, and land cover classification, HSI is increasingly applied in medical imaging due to its ability to detect subtle biochemical and structural variations beyond the capabilities of conventional modalities [1]. By integrating spatial and spectral information, HSI supports precise tissue analysis for tasks such as tumor detection, vascular visualization, and histopathological segmentation [2]. The combination with advanced computational methods has further improved feature extraction and diagnostic performance [3].

Despite these advances, the integration of HSI with deep learning introduces vulnerability to adversarial attacks—small, imperceptible perturbations that can severely mislead models [4]. This is especially concerning in medical applications, where misclassification may compromise patient safety [5]. Studies on diabetic retinopathy grading and Alzheimer’s disease prediction confirm that minor perturbations can cause significant performance drops [6]. HSI models, which rely on rich spectral-spatial features, are particularly susceptible to such attacks [7].

In hyperspectral remote sensing, CNN-based models dominate classification tasks due to their ability to process high-

dimensional data and learn complex spectral-spatial features [8]. Existing adversarial attacks mainly focus on pixel-level perturbations, assuming classification depends only on spectral information from individual pixels. However, in hyperspectral medical images, spatial dependencies between neighboring pixels are critical [9]. Tissue structure and tumor boundaries are often defined by local spatial patterns, and minor local variations can significantly affect classification [10]. As a result, current adversarial methods often underperform in medical HSI (MHSI), where such spatial context is indispensable.

Furthermore, compared with remote sensing, MHSI contains more complex and Multiscale information. Medical images are smaller in spatial scale but demand higher resolution to distinguish subtle variations in tissue, vasculature, and abnormalities [11]. Fine-grained tumor characteristics require local-scale analysis, while broader structures such as vascular networks benefit from global-scale interpretation [1]. Unlike remote sensing imagery focused on large-scale patterns [12], MHSI involves intricate Multiscale features essential for accurate diagnosis [13].

Despite progress, most adversarial methods overlook these characteristics, focusing solely on spectral or pixel-level perturbations [14]. This gap limits their effectiveness in medical contexts and calls for more tailored attack strategies that exploit spatial dependencies and Multiscale information.

In this paper, our main contributions are as follows:

- We identify the unique vulnerabilities of MHSI models stemming from local pixel dependencies and Multiscale spectral-spatial structures.
- We propose two novel attack methods: **Local Pixel Dependency Attack** and **Multiscale Information Attack**, designed to exploit these characteristics.
- We demonstrate through experiments that our methods substantially reduce classification accuracy in critical regions while preserving perturbation imperceptibility, highlighting the urgent need for dedicated defense mechanisms.

II. RELATED WORKS

A. Hyperspectral Image Classification

Hyperspectral image classification has progressed from traditional methods (PCA, SVM, KNN) to deep learning approaches that automate feature extraction and integrate

spectral-spatial information [15]. While computationally efficient, traditional methods require extensive feature engineering for high-dimensional data [16]. Convolutional Neural Networks (CNNs) significantly advanced the field by exploiting spectral-spatial correlations. Early 2D-CNNs extracted spatial features, while 3D-CNNs enabled spectral-spatial integration. Hybrid architectures like HybridSN balance efficiency and accuracy through combined 3D-2D convolutions [17]. The Spectral-Spatial Residual Network(SSRN) further improved generalization via residual learning [18]. The Self-attention Context Network(SACNet) employs self-attention and context encoding to capture global dependencies, improving robustness through hierarchical feature extraction [19].

B. Medical Hyperspectral Image Classification

Medical HSI (MHSI) classification provides critical diagnostic insights but faces high-dimensionality challenges. CNN-based methods effectively capture hierarchical spectral-spatial features and have been widely applied to tumor and lesion analysis [20]. Recent works emphasize the importance of pixel dependencies and multiscale structures, demonstrating that accurate modeling of local spatial coherence and hierarchical spectral-spatial patterns is crucial for robust medical diagnosis under perturbations [10], [13]. More recently, the Dual-Stream model has been introduced for medical hyperspectral classification, integrating complementary spatial and spectral streams to enhance discriminative power [21].

C. Adversarial Attack and Defense on Hyperspectral Images

Adversarial attacks exploit imperceptible perturbations to induce misclassification. For hyperspectral data, several representative attack methods have been developed. Spectral-Spatial FGSM(SS-FGSM) perturbs spectral features at the pixel level [22], while Spectral-Spatial Attack(SSA) explores spectral-spatial adversarial strategies [23]. Multifeature collaborative adversarial Network(MfcaNet) introduces multi-feature collaborative perturbations to enhance attack success rates [14]. These approaches, however, were not specifically designed for medical HSI, leaving vulnerabilities in clinical applications.

In parallel, defense networks have been proposed to counter such threats. The Robust Class Context-Aware(RCCA) network leverages contextual class dependencies to enhance robustness against adversarial perturbations [24]. The Weighted Fusion of Spectral Transformer and Spatial Self-Attention(WFSS) integrates transformer-based spectral modeling with spatial self-attention for multi-level defense [25]. More recently, attention-based defenses such as Attack-Invariant Attention Feature(AIAF) and Spatial-spectral self-attention Network(S³ANet) have been introduced, focusing on adaptive information aggregation and spectral-spatial alignment to suppress adversarial noise while preserving lesion structures [26], [27]. These methods represent strong defensive baselines, and we include them in our experiments to comprehensively evaluate the effectiveness of our proposed attack framework.

III. METHOD

A. Local Pixel Dependency Attack

Medical hyperspectral images exhibit strong spatial dependencies among neighboring pixels, which are critical for preserving tissue structure. We exploit this property and propose the *Local Pixel Dependency Attack* to generate imperceptible yet effective adversarial examples by incorporating local pixel correlations into gradient-based perturbations.

Given an input hyperspectral image \mathbf{x} with ground-truth label y , we compute the gradient of the loss function \mathcal{L} with respect to \mathbf{x} :

$$\nabla_{\mathbf{x}} \mathcal{L}(\mathbf{x}, y). \quad (1)$$

Instead of perturbing each pixel independently, we average gradients within a local window $\mathcal{W}(i, j)$ to preserve spatial coherence. The adversarial example is generated as:

$$\mathbf{x}_{\text{adv}} = \mathbf{x} - \varepsilon \cdot \frac{1}{N_{i,j}} \sum_{(i',j') \in \mathcal{W}(i,j)} \nabla_{\mathbf{x}} \mathcal{L}(\mathbf{x}, y), \quad (2)$$

where ε controls the perturbation magnitude and $N_{i,j}$ denotes the number of pixels in the local window.

The attack is applied iteratively:

$$\mathbf{x}^{(t+1)} = \mathbf{x}^{(t)} - \varepsilon \cdot \frac{1}{N_{i,j}} \sum_{(i',j') \in \mathcal{W}(i,j)} \nabla_{\mathbf{x}} \mathcal{L}(\mathbf{x}^{(t)}, y), \quad (3)$$

typically for 20 iterations, enabling gradual misclassification while maintaining spatial consistency.

For targeted attacks, the objective is modified to force prediction toward a specific target label \hat{y} :

$$\mathcal{L}(\mathbf{x}_{\text{adv}}, \hat{y}) = -\log P(\hat{y} | \mathbf{x}_{\text{adv}}). \quad (4)$$

B. Multiscale Information Attack

Hyperspectral images exhibit strong multiscale spectral-spatial dependencies. To exploit this property, we propose the *Multiscale Information Attack*, which generates adversarial perturbations across multiple spatial resolutions via downsampling and upsampling operations.

Given an input hyperspectral image $\mathbf{x} \in \mathbb{R}^{B \times D \times H \times W}$, for each scale $s \in \mathcal{S}$ and spectral band $\mathbf{x}^{(d)}$, we first apply downsampling:

$$\mathbf{x}_{\text{down}}^{(d,s)} = \text{Downsample}(\mathbf{x}^{(d)}, s). \quad (5)$$

At the downsampled resolution, gradient-based perturbations are added:

$$\mathbf{x}_{\text{pert}}^{(d,s)} = \mathbf{x}_{\text{down}}^{(d,s)} + \varepsilon \cdot \nabla_{\mathbf{x}_{\text{down}}^{(d,s)}} \mathcal{L}(\mathbf{x}, y), \quad (6)$$

where ε controls the perturbation magnitude. The perturbed features are then upsampled to the original spatial size:

$$\mathbf{x}_{\text{up}}^{(d,s)} = \text{Upsample}(\mathbf{x}_{\text{pert}}^{(d,s)}, (H, W)). \quad (7)$$

For each scale s , perturbations are aggregated across spectral bands:

$$\mathbf{p}_s = \sum_{d=1}^D \mathbf{x}_{\text{up}}^{(d,s)}. \quad (8)$$

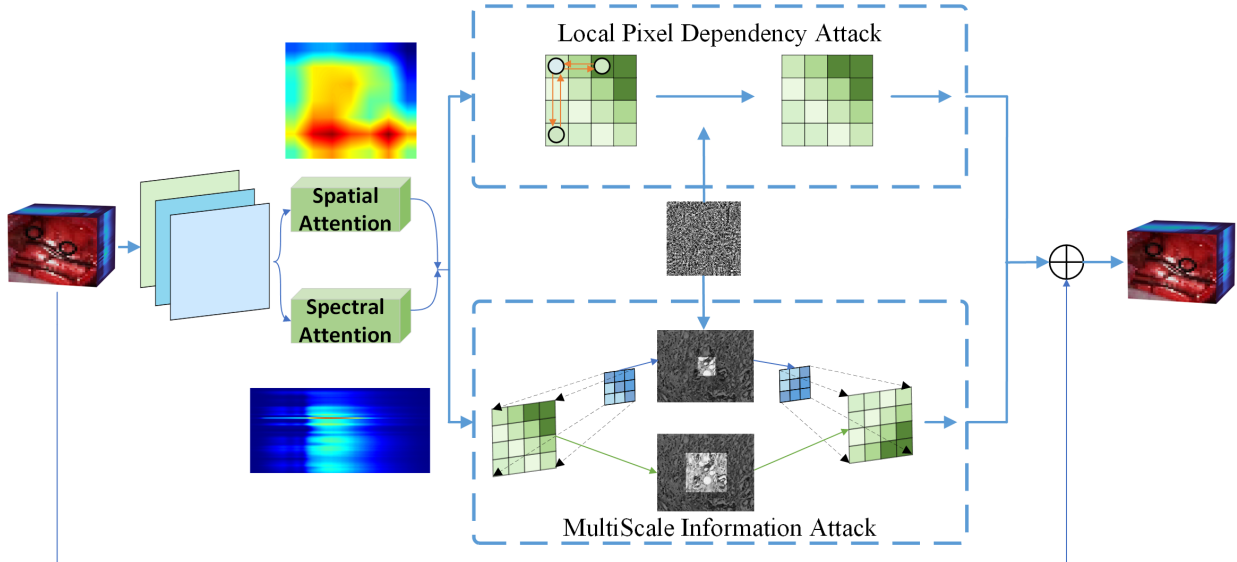


Fig. 1: The proposed adversarial attack and defense framework for HSI classification.

The final multiscale perturbation is obtained by summing over all scales:

$$\mathbf{p} = \sum_{s \in \mathcal{S}} \mathbf{p}_s. \quad (9)$$

The adversarial example is generated as:

$$\mathbf{x}_{\text{adv}} = \mathbf{x} + \varepsilon \cdot \mathbf{p}. \quad (10)$$

C. Adversarial Attack Framework

The final adversarial perturbation is the combination of the local pixel-dependent perturbation and the Multiscale perturbation:

$$\delta_{\text{final}} = \delta_{\text{local}} + \delta_{\text{Multiscale}} \quad (11)$$

The adversarial example is then generated as:

$$\mathbf{x}_{\text{adv}} = \mathbf{x} + \delta_{\text{final}}, \quad (12)$$

where \mathbf{x} is the original hyperspectral image, and \mathbf{x}_{adv} is the perturbed adversarial example.

IV. EXPERIMENTS

A. Datasets

1) *In-Vivo Hyperspectral Human Brain Image Database for Brain Cancer Detection*: The In-Vivo Hyperspectral Human Brain Image Database for Brain Cancer Detection consists of 36 hyperspectral images collected from 22 neurosurgical operations [28]. It covers four annotated classes: normal tissue, tumor tissue, blood vessels, and background elements. The images span the Visual and Near-Infrared (VNIR) spectrum from 400 to 1000 nm, providing over 300,000 labeled spectral signatures. Labels were generated using a semi-automatic methodology based on the Spectral Angle Mapper (SAM) algorithm, cross-referenced with histopathological evaluations. This dataset serves as a significant resource for developing machine learning models for brain tumor classification and guiding real-time surgical decisions.

2) *MultiDimensional Choledoch (MDC) Dataset*: Multi-Dimensional Choledoch (MDC) Dataset includes 880 hyperspectral scenes collected from 174 individuals, comprising 689 scenes with partial cancer regions (L), 49 with complete cancerous areas (N), and 142 without cancer (P) [29]. This dataset only uses binary classification to determine the cancer region from the normal region. The hyperspectral data were captured using a system with a 20x objective lens, covering wavelengths from 450 nm to 1000 nm with 60 spectral bands per scene. Each hyperspectral image was resized to 256x320 pixels to enhance computational efficiency.

B. Experimental Setup

In this study, we performed experiments on hyperspectral image datasets, specifically targeting medical image classification tasks. To reduce the data dimensionality and extract the most important spectral features, Principal Component Analysis (PCA) was applied, reducing the spectral dimensions to 20 components. This reduction in dimensionality helps minimize computational overhead while retaining the essential spectral information for classification.

For data preprocessing, image cubes were generated using a sliding window approach with a window size of 11x11, allowing for the extraction of local spatial-spectral features. Zero-padding was applied at the borders to handle edge pixels, which do not have enough neighboring pixels for patch extraction. We used a training-to-testing split of 80% for training and 20% for testing, ensuring that the training set included a diverse representation of different classes.

C. Evaluation Metrics

In medical image adversarial attacks, misclassifying lesion regions as normal tissue poses the greatest clinical risk. Therefore, we primarily evaluate the attack success rate on lesion areas, where a lower classification accuracy indicates

target model	attack method	Normal Tissue(↓)	Tumor Tissue(↑)	Hyper vascularized(↓)	Background(↓)	OA	AA	KAPPA	L0	L2
HybridSN [17]	MfcaNet [14]	0	85.81	0	0	96.61	78.45	95.02	3428	12.2
	SSA [23]	0	86.53	0	0	96.61	78.42	95.01	4687	13.6
	SS-FGSM [22]	0	82.16	0	0	96.61	78.44	95.02	3274	11.3
	Ours	0	92.02	0	0	96.59	78.3	94.98	1896	7.8
SSRN [18]	MfcaNet [14]	0	85.25	0	0	96.61	78.47	95.03	3512	12.5
	SSA [23]	0	78.14	0	0	96.63	78.68	95.08	4825	14.1
	SS-FGSM [22]	0	88.06	0	0	96.6	78.32	95.03	3341	11.5
	Ours	0	95.35	0	0	96.58	78.9	94.95	1958	8.1
SacNet [19]	MfcaNet [14]	0	81.72	0	0	96.62	78.57	95.05	3395	11.9
	SSA [23]	0	74.33	0	0	96.64	78.82	95.12	4973	14.7
	SS-FGSM [22]	0	83.46	0	0	96.62	78.51	95.04	3189	11
	Ours	0	91.54	0	0	96.59	78.32	94.99	2027	8.5
Dual-Stream [21]	MfcaNet [14]	0	71.41	0	0	96.68	82.15	94.22	3607	13
	SSA [23]	0	67.66	0	0	95.8	83.09	93.75	4896	14.4
	SS-FGSM [22]	0	62.55	0	0	95.96	84.36	94.46	3425	11.8
	Ours	0	80.75	0	0	95.48	79.81	92.48	2144	8.7
RCCA [24]	MfcaNet [14]	0.45	16.39	0.17	0.06	99.09	95.54	98.55	2968	10.4
	SSA [23]	1.73	24.18	0.39	0.63	98.31	93.27	96.91	4087	11.9
	SS-FGSM [22]	0.42	20.86	0.11	0.45	98.72	94.68	97.08	2854	10.9
	Ours	1.22	31.41	0.69	1.25	97.94	92.95	95.28	1718	7
WFSS [25]	MfcaNet [14]	1.17	28.02	0.58	0.42	98.07	93.45	98.04	2897	10.7
	SSA [23]	0.88	17.96	0.03	0.09	98.93	95.29	98.97	4149	12.2
	SS-FGSM [22]	1.28	32.05	0.85	1.15	97.86	93.16	95.13	2766	10.8
	Ours	1.28	37.68	1.37	1.63	96.91	90.76	93.57	1684	6.8
AIAF [26]	MfcaNet [14]	0.3	14.8	0.04	0.08	98.72	96.22	98.25	3021	10.9
	SSA [23]	1.1	18.55	0.37	0.29	98.39	94.94	97.62	4012	11.7
	SS-FGSM [22]	0.38	16.88	0.2	0.12	98.63	95.64	98.02	2879	11
	Ours	0.85	29.66	1.03	0.79	98.01	91.87	96.62	1741	7.1
S ³ ANet [27]	MfcaNet [14]	0.26	13.98	0.09	0.02	98.77	96.34	98.31	2954	10.6
	SSA [23]	0.8	17.43	0.33	0.39	98.46	95.43	97.73	4193	12.1
	SS-FGSM [22]	0.35	15.7	0.16	0.24	98.66	95.96	98.08	2798	10.7
	Ours	0.82	27.89	0.87	1.09	98.1	92.81	96.8	1697	6.9

TABLE I: Performance Comparison of Adversarial Attacks on the Brain Dataset Across Different Models.

a more effective attack. In addition, we adopt three standard metrics for comprehensive evaluation.

Overall Accuracy (OA) measures the proportion of correctly classified pixels:

$$OA = \frac{\sum_{i=1}^C N_{ii}}{\sum_{i=1}^C \sum_{j=1}^C N_{ij}}, \quad (13)$$

where N_{ij} denotes the number of pixels with ground-truth class i predicted as class j , and C is the number of classes.

Average Accuracy (AA) evaluates class-balanced performance:

$$AA = \frac{1}{C} \sum_{i=1}^C \frac{N_{ii}}{\sum_{j=1}^C N_{ij}}. \quad (14)$$

Cohen's Kappa measures the agreement between predictions and ground truth while accounting for chance:

$$\kappa = \frac{p_o - p_e}{1 - p_e}, \quad (15)$$

where

$$p_o = \frac{\sum_{i=1}^C N_{ii}}{\sum_{i=1}^C \sum_{j=1}^C N_{ij}}, \quad p_e = \sum_{i=1}^C \left(\frac{\sum_j N_{ij}}{\sum_{i,j} N_{ij}} \cdot \frac{\sum_j N_{ji}}{\sum_{i,j} N_{ij}} \right). \quad (16)$$

These metrics jointly assess overall accuracy, class balance, and statistical reliability under adversarial conditions.

D. Results Under Attacks and Defenses

We jointly analyze the results on the Brain dataset (Table I) and the MDC dataset (Table II) to provide a unified, mechanism-oriented evaluation across datasets and architectures. The experiments cover multiple baseline classifiers (HybridSN, SSRN, SACNet, Dual-Stream) as well as representative defense-oriented networks (RCCA, WFSS, AIAF, and S³ANet), enabling consistent cross-model observations.

A consistent lesion-first degradation pattern is observed across all settings. While global metrics such as OA, AA, and Kappa remain high—typically above 96% under defense models—the accuracy of lesion-related classes (tumor or cancer) drops sharply under our attack. For instance, under WFSS, tumor accuracy on the Brain dataset decreases to 37.68%, and cancer accuracy on the MDC dataset decreases to 54.73%, despite near-saturated global performance. This discrepancy reflects a clinically critical failure mode in which false negatives are amplified while overall accuracy appears unaffected.

target model	attack method	Normal (\downarrow)	Cancer (\uparrow)	OA	AA	KAPPA	L0	L2
HybridSN [17]	MfcaNet [14]	0	84.21	87.11	57.9	69.47	1428	13.5
	SSA [23]	0	76.83	88.29	61.59	73.91	1764	13.9
	SS-FGSM [22]	0	81.54	87.69	59.23	71.08	1289	11.7
	Ours	0	89.69	86.55	55.16	66.47	752	7.8
SSRN [18]	MfcaNet [14]	0	83.46	87.38	58.27	69.96	1387	12.8
	SSA [23]	0	72.72	89.09	63.64	76.36	1721	13.4
	SS-FGSM [22]	0	71.43	89.29	64.29	77.14	1244	11.2
	Ours	0	86.38	87.72	56.81	68.17	713	7.4
SacNet [19]	MfcaNet [14]	0	84.51	87.09	57.75	69.3	1472	13.9
	SSA [23]	0	80.57	87.72	59.72	71.65	1802	14.3
	SS-FGSM [22]	0	86.19	86.91	56.91	68.27	1326	12
	Ours	0	90.44	86.39	54.78	65.74	794	8.2
Dual-Stream [21]	MfcaNet [14]	0	57.85	92.86	71.08	85.75	1398	13.1
	SSA [23]	0	62.13	92	68.94	83.25	1750	13.6
	SS-FGSM [22]	0	54.06	93.06	72.97	86.29	1279	11.6
	Ours	0	67.36	91.64	66.32	82.35	741	7.6
RCCA [24]	MfcaNet [14]	0.4	47.29	92.68	71.36	85.03	1194	11
	SSA [23]	0.67	51.48	92	68.91	83.2	1532	11.2
	SS-FGSM [22]	0.3	43.63	93.09	72.69	86.17	1093	10.3
	Ours	1.09	55.32	91.23	66.34	81.77	624	6.9
WFSS [25]	MfcaNet [14]	0.48	46.98	92.76	71.51	85.16	1181	10.8
	SSA [23]	0.82	50.86	92.12	69.07	83.36	1519	11.1
	SS-FGSM [22]	0.32	42.89	93.17	73.56	86.62	1085	10.1
	Ours	1.14	54.73	91.33	66.64	82.11	611	6.7
AIAF [26]	MfcaNet [14]	0.5	25.5	94.88	86.75	92.18	1042	9.7
	SSA [23]	0.86	29.7	94.21	84.72	90.95	1379	10
	SS-FGSM [22]	0.34	21.75	95.25	88.88	93.17	987	9.1
	Ours	1.21	33.88	93.64	82.46	89.15	552	6.2
S ³ ANet [27]	MfcaNet [14]	0.58	24.97	94.93	87.02	92.39	1026	9.5
	SSA [23]	0.91	28.93	94.27	85.04	91.04	1364	9.8
	SS-FGSM [22]	0.36	20.94	95.32	89.53	93.44	972	9
	Ours	1.15	32.74	93.96	83.13	89.89	543	6.1

TABLE II: Performance Comparison of Adversarial Attacks on the MDC Dataset Across Different Models.

Across baseline classifiers, the effect is even more pronounced. On the Brain dataset, tumor misclassification rates reach 92.02% for HybridSN, 95.35% for SSRN, and 91.54% for SACNet, reducing tumor accuracy to single-digit levels. The particularly severe degradation on SSRN suggests that models relying on residual spectral–spatial coupling are highly vulnerable to locally coherent, multiscale perturbations that induce boundary shifts in lesion regions.

On the MDC dataset, a similar targeted behavior is observed. Normal tissue accuracy remains at 100% across all baseline classifiers, whereas cancer samples experience substantial degradation, with misclassification rates of 89.69%, 86.38%, 90.44%, and 67.36% for HybridSN, SSRN, SACNet, and Dual-Stream, respectively. This asymmetric shift from positive (cancer) to negative (normal) predictions corresponds to the most harmful clinical error mode.

Defense-oriented networks improve robustness in terms

of global accuracy but remain vulnerable to targeted perturbations. Under RCCA and WFSS, Brain tumor accuracy decreases to 31.41% and 37.68%, respectively, while MDC cancer accuracy drops to 55.32% and 54.73%. Similar trends are observed for AIAF and S³ANet, where tumor accuracy on Brain falls below 30%, and cancer accuracy on MDC approaches 33%. These results indicate that existing defenses primarily preserve average performance rather than safeguarding clinically critical lesion classes.

These observations align with the design of our attack. The local pixel dependency component enforces spatial coherence by averaging gradients within neighborhoods, while the multiscale component perturbs representations across resolutions and reprojects them to the original scale. Together, they induce targeted decision boundary shifts in lesion regions without introducing conspicuous artifacts, explaining the coexistence of high global metrics and severe lesion-class collapse. s.

V. DISCUSSION

This study introduces a specialized adversarial attack framework specifically designed for medical hyperspectral imaging, addressing the unique spectral-spatial characteristics and Multiscale features inherent in medical data. Our innovative Local Pixel Dependency Attack leverages precise spatial relationships between neighboring pixels, while the Multiscale Information Attack strategically targets hierarchical spectral-spatial features. These innovations effectively exploit critical vulnerabilities in medical deep learning classifiers, significantly reducing classification accuracy for clinically relevant tumor regions on Brain and MDC datasets, outperforming existing methods such as SS-FGSM, SSA, and MfcaNet. However, our approach could be further enhanced by incorporating domain-specific priors, such as spectral similarity between tumor and surrounding tissues, to refine perturbation precision.

The clinical relevance of our method is substantial, as adversarial misclassifications of tumor regions can critically affect diagnostic accuracy, leading to potential misdiagnoses and compromised patient outcomes. By explicitly addressing vulnerabilities related to spectral-spatial dependencies and Multiscale information, this research highlights the urgent need for robust defensive strategies tailored specifically to medical HSI-based diagnostic systems. Future research will validate clinical applicability in diverse scenarios and develop targeted defenses to enhance medical imaging reliability.

REFERENCES

- [1] Guolan Lu and Baowei Fei, "Medical hyperspectral imaging: a review," *Journal of biomedical optics*, vol. 19, no. 1, pp. 010901–010901, 2014.
- [2] Guolan Lu, Luma Halig, Dongsheng Wang, Xulei Qin, Zhuo Georgia Chen, and Baowei Fei, "Spectral-spatial classification for noninvasive cancer detection using hyperspectral imaging," *Journal of biomedical optics*, vol. 19, no. 10, pp. 106004–106004, 2014.
- [3] Rong Cui, He Yu, Tingfa Xu, Xiaoxue Xing, Xiaorui Cao, Kang Yan, and Jiexi Chen, "Deep learning in medical hyperspectral images: A review," *Sensors*, vol. 22, no. 24, pp. 9790, 2022.
- [4] Daya Kumar, Abhijith Sharma, and Apurva Narayan, "Attacking cnns in histopathology with snap: sporadic and naturalistic adversarial patches (student abstract)," in *Proceedings of the AAAI Conference on Artificial Intelligence*, 2024, vol. 38, pp. 23550–23551.
- [5] Ian J Goodfellow, Jonathon Shlens, and Christian Szegedy, "Explaining and harnessing adversarial examples," *arXiv preprint arXiv:1412.6572*, 2014.
- [6] İnci M Baytas, "Predicting progression from mild cognitive impairment to alzheimer's dementia with adversarial attacks," *IEEE Journal of Biomedical and Health Informatics*, 2024.
- [7] Weijia Zeng, Wei Li, Mengmeng Zhang, Hao Wang, Meng Lv, Yue Yang, and Ran Tao, "Microscopic hyperspectral image classification based on fusion transformer with parallel cnn," *IEEE Journal of Biomedical and Health Informatics*, vol. 27, no. 6, pp. 2910–2921, 2023.
- [8] Muhammad Jaleed Khan, Hamid Saeed Khan, Adeel Yousaf, Khurshid, and Asad Abbas, "Modern trends in hyperspectral image analysis: A review," *Ieee Access*, vol. 6, pp. 14118–14129, 2018.
- [9] Uzair Khan, Sidiq Paheding, Colin P Elkin, and Vijaya Kumar Devabhaktuni, "Trends in deep learning for medical hyperspectral image analysis," *IEEE Access*, vol. 9, pp. 79534–79548, 2021.
- [10] Xingran Xie, Ting Jin, Boxiang Yun, Qingli Li, and Yan Wang, "Exploring hyperspectral histopathology image segmentation from a deformable perspective," in *Proceedings of the 31st ACM International Conference on Multimedia*, 2023, pp. 242–251.
- [11] Baowei Fei, "Hyperspectral imaging in medical applications," in *Data handling in science and technology*, vol. 32, pp. 523–565. Elsevier, 2019.
- [12] Danyang Peng, Haoran Feng, Jun Wu, Yi Wen, Tingting Han, Yuanyuan Li, Guangyu Yang, and Lei Qu, "Robust hyperspectral image classification using a multi-scale transformer with long-short-distance spatial-spectral cross-attention," *IEEE Transactions on Geoscience and Remote Sensing*, 2024.
- [13] Xueling Wei, Wei Li, Mengmeng Zhang, and Qingli Li, "Medical hyperspectral image classification based on end-to-end fusion deep neural network," *IEEE Transactions on Instrumentation and Measurement*, vol. 68, no. 11, pp. 4481–4492, 2019.
- [14] Cheng Shi, Yenan Dang, Li Fang, Minghua Zhao, Zhiyong Lv, Qiguang Miao, and Chi-Man Pun, "Multifeature collaborative adversarial attack in multimodal remote sensing image classification," *IEEE Transactions on Geoscience and Remote Sensing*, vol. 60, pp. 1–15, 2022.
- [15] Shutao Li, Weiwei Song, Leyuan Fang, Yushi Chen, Pedram Ghamisi, and Jon Atli Benediktsson, "Deep learning for hyperspectral image classification: An overview," *IEEE Transactions on Geoscience and Remote Sensing*, vol. 57, no. 9, pp. 6690–6709, 2019.
- [16] Brajesh Kumar, Onkar Dikshit, Ashwani Gupta, and Manoj Kumar Singh, "Feature extraction for hyperspectral image classification: A review," *International Journal of Remote Sensing*, vol. 41, no. 16, pp. 6248–6287, 2020.
- [17] Swalpa Kumar Roy, Gopal Krishna, Shiv Ram Dubey, and Bidyut B Chaudhuri, "Hybridsn: Exploring 3-d-2-d cnn feature hierarchy for hyperspectral image classification," *IEEE Geoscience and Remote Sensing Letters*, vol. 17, no. 2, pp. 277–281, 2019.
- [18] Zilong Zhong, Jonathan Li, Zhiming Luo, and Michael Chapman, "Spectral-spatial residual network for hyperspectral image classification: A 3-d deep learning framework," *IEEE Transactions on Geoscience and Remote Sensing*, vol. 56, no. 2, pp. 847–858, 2017.
- [19] Yonghao Xu, Bo Du, and Liangpei Zhang, "Self-attention context network: Addressing the threat of adversarial attacks for hyperspectral image classification," *IEEE Transactions on Image Processing*, vol. 30, pp. 8671–8685, 2021.
- [20] Qian Huang, Wei Li, Baochang Zhang, Qingli Li, Ran Tao, and Nigel H Lovell, "Blood cell classification based on hyperspectral imaging with modulated gabor and cnn," *IEEE journal of biomedical and health informatics*, vol. 24, no. 1, pp. 160–170, 2019.
- [21] Boxiang Yun, Qingli Li, Lubov Mitrofanova, Chunhua Zhou, and Yan Wang, "Factor space and spectrum for medical hyperspectral image segmentation," in *International Conference on Medical Image Computing and Computer-Assisted Intervention*. Springer, 2023, pp. 152–162.
- [22] Cheng Shi, Mengxin Zhang, Zhiyong Lv, Qiguang Miao, and Chi-Man Pun, "Universal object-level adversarial attack in hyperspectral image classification," *IEEE Transactions on Geoscience and Remote Sensing*, vol. 61, pp. 1–14, 2023.
- [23] Zhaoxia Yin, Lichun Tang, Cong Kong, Hang Su, and Bin Luo, "Sparse adversarial attack method for deep learning hyperspectral image classification models," CN Patent: CN117079137B, 2025, Granted patent.
- [24] Bing Tu, Wangquan He, Qianming Li, Yishu Peng, and Antonio Plaza, "A new context-aware framework for defending against adversarial attacks in hyperspectral image classification," *IEEE Transactions on Geoscience and Remote Sensing*, vol. 61, pp. 1–14, 2023.
- [25] Lichun Tang, Zhaoxia Yin, Hang Su, Wanli Lyu, and Bin Luo, "Wfss: weighted fusion of spectral transformer and spatial self-attention for robust hyperspectral image classification against adversarial attacks," *Visual Intelligence*, vol. 2, no. 1, pp. 5, 2024.
- [26] Cheng Shi, Ying Liu, Minghua Zhao, Chi-Man Pun, and Qiguang Miao, "Attack-invariant attention feature for adversarial defense in hyperspectral image classification," *Pattern Recognition*, vol. 145, pp. 109955, 2024.
- [27] Yichu Xu, Yonghao Xu, Hongzan Jiao, Zhi Gao, and Lefei Zhang, "S³anet: Spatial-spectral self-attention learning network for defending against adversarial attacks in hyperspectral image classification," *IEEE Transactions on Geoscience and Remote Sensing*, vol. 62, pp. 1–13, 2024.
- [28] Himar Fabelo, Samuel Ortega, Adam Szolnai, Diederik Bulters, Juan F Piñeiro, Silvester Kabwama, Aruma JO'Shanahan, Harry Bulstrode, Sara Bisschopp, B Ravi Kiran, et al., "In-vivo hyperspectral human brain image database for brain cancer detection," *IEEE Access*, vol. 7, pp. 39098–39116, 2019.
- [29] Qing Zhang, Qingli Li, Guanzen Yu, Li Sun, Mei Zhou, and Junhao Chu, "A multidimensional choledoch database and benchmarks for cholangiocarcinoma diagnosis," *IEEE access*, vol. 7, pp. 149414–149421, 2019.